Journal of Cancer Therapy, **2009, 1, 19-27**
Published Online September 2009 in SciRes (www.SciRP.org/journal/cancer)

Conformal Microwave Imaging for Breast Cancer Detection

ABSTRACT

An important feature of our Gauss–Newton iterative scheme for microwave breast image reconstruction is that only the heterogeneous target zone within the antenna array is represented using the finite-element method, while the surrounding homogeneous coupling medium is modeled with the boundary-element (BE) method. The interface between these two zones may be arbitrary in shape and position with the restriction that the BE region contains only the homogeneous coupling liquid. In this paper, we demonstrate through simulation and phantom experiments, as well as in patient examinations, that the detection of tumor inclusions can be enhanced as the target zone approaches the exact breast perimeter. It is also shown that central artifacts that often appear in the reconstructed images that may potentially confound the ability to distinguish benign and malignant conditions have also been reduced.

***Keywords*:** *Background contrast, breast, conformal mesh, microwave imaging.*

1. Introduction

AMERICAN cancer statistics indicate that breast cancer is the most common nonskin malignancy in women and the second leading cause of female cancer mortality [1]. One of the important strategies for increasing the likelihood of successful treatment and long-term survival is the detection of breast tumors at an early stage. Although recognized currently as the most effective tool for screening breast cancer, X-ray mammography still suffers from a high callback rate of roughly 11% [2] and a significant false-negative detection rate, ranging from 4% to 34% [3]. Alternative imaging modalities that produce functional information about the breast in terms of tissue property distributions are being developed in an effort to improve detection and reduce unnecessary biopsies. For instance, a study is being conducted for breast cancer detection at Dartmouth College, Hanover, NH, which includes four different modalities, i.e., microwave imaging spectroscopy (MIS), electrical impedance spectroscopy (EIS), near infrared imaging (NIR), and magnetic resonance elastrography (MRE). Due to significant contrasts between normal and malignant tissue available for these imaging modalities [8–12], diagnoses may be enhanced considerably with their use.

Among the early studies on microwave imaging, passive radiometric detection of the thermal emissions associated with nonpalpable breast tumors has been studied and has demonstrated a positive predictive value when combined with mammography to reduce noncancerous breast biopsies [13,14]. For active microwave breast imaging, confocal microwave imaging has been studied in simulation for the application of active ultra-wide-band backscatter microwave radar technology in breast imaging [15,16]. Near-field model-based imaging techniques have achieved encouraging results in simulation, laboratory scale experiments, and preliminary clinical exams [17–20]. Initial exams on a small number of volunteer subjects reported by Meaney *et al*. [4] have successfully demonstrated the recovery of breast electrical properties at microwave frequencies using a model-based image-reconstruction approach.

An important feature of this imaging technique is that the model for the forward solution portion of the reconstruction algorithm is a coupling of two numerical approaches representing two separate two-dimensional (2-D) zones. The first zone is the target region located within the antenna array and is conveniently modeled using a finite-element (FE) approach because of its heterogeneous nature during the reconstruction process [21]. (In terms of the inverse procedure, a more coarse reconstruction mesh is superimposed over this grid [22].) The second zone is the homogenous space surrounding the target region, which encompasses the antenna array elements and extends to infinity. This is conveniently represented with the boundary-element (BE) method and requires discretization of only the integration path along the FE mesh boundary [21]. Coupling of these two solutions provides an efficient and accurate approach to compute the forward solution without unnecessary FE discretization of space beyond the target zone and without dependence on approximate boundary conditions, respectively.

Exploiting the flexible nature of this representation, the

FE mesh can assume any arbitrary shape and position within the array. For general imaging purposes, defining the target zone as a full concentric space within the circular antenna array is appropriate. However, for site-specific applications such as breast imaging, it may prove useful to conform the FE and property reconstruction meshes to the exact breast perimeter. In principle, this allows for a property step function to be imposed in the forward model (the algorithm assumes a homogeneous property distribution outside of the target region) [21] at the breast/background medium interface. It also facilitates deployment of all reconstruction parameter nodes to locations only within the breast, as opposed to some occupying space corresponding to the coupling medium where the property values are already known. Implementation of this idea requires two steps—defining the imaging target boundary and reconstructing the image within the conformed boundary. In this paper, we focus on the latter by examining the feasibility of conforming the imaging zone to known boundaries (e.g., simulated or exper- imental phantomswith known sizes and positions).We study the effects on image quality as a function of the mesh approaching the exact object perimeter as a way of assessing how accurately the object boundary must be known. Results from an actual clinical case are also presented using this technique with the breast– coupling-medium interface identified from the reconstructed image for the same exam data utilizing a fixed circular target zone. Enhanced images with respect to tumor detection demonstrate the benefits of this approach.

Interestingly, recent homogeneous simulation and phantom imaging experiments with this approach have exhibited some unwanted artifacts within the reconstructed object. It is important that artifacts be minimized so that they do not obscure diagnostically relevant features or falsely indicate nonexistent abnormalities. A numerical study described in the final portion of this paper demonstrates that these artifacts can be significantly diminished by reducing the background/breast electrical property contrast.

2. METHOD

2.1. Imaging Reconstruction Scheme

We recover the relative permittivity and conductivity distributions of the imaging object using a Gauss–Newto-n iterative scheme, which minimizes the squared difference between the TM electric-field measurements and the field values calculated by a 2-D scalar full-wave computational model (forward solution) [23]. Our existing forward algorithm divides the modeling task into two natural partitions, i.e., the heterogeneous imaging zone and homogeneous surrounding region with the exact interface being somewhat arbitrarily defined. The electric-field distribution for combined areas is obtained through a hybrid of the FE method for the target region and the BE method for the surrounding homogeneous zone, respectively, which are coupled to form a complete forwa- rd-solution hybrid-element (HE) method [21]. An important feature of this forward model approach is the elimination of approximate boundary conditions. The appr- oach is also efficient since the FE mesh is discretized over a relatively small space and the discretization of the BE region is only required about the perimeter of the FE grid. The antennas are positioned within the BE region where all electrical properties and transmit–receive characteristics remain constant during the reconstruction process. In order to reduce the number of reconstruction parameters while maintaining computational accuracy in the forward solution, we have applied a dual-mesh scheme to the reconstruction algorithm, where the electric property distribution is recovered on a less densely discretized mesh superimposed exactly over the FE zone mesh [22].

A fundamental requirement for the HE approach to produce an accurate solution of unbounded electromagnetic field propagation problem is that the BE zone should contain only homogenous saline and no portion of the imaging object. With this condition met, the actual FE grid and associated dual (property) mesh can be constructed in any shape and positioned arbitrarily within the antenna array. The electric fields computed within the area of interest (e.g., imaging target) on different FE meshes do not change, except possibly for slight improvements in accuracy since the mesh is more densely discretized over the smaller zone. This provides the opportunity to conform the FE mesh perimeter exactly to the object boundary in the ideal situation, and essentially maximizes the number of parameter nodes used to represent the object.

In our iterative image-reconstruction scheme, we have also employed a filtering of the recovered image to reduce undesired high-frequency spatial variation [24]. This effectively prevents the algorithm from converging to an unwanted local minimum; however, it significantly reduces the spatial resolution by smoothing the coupling medium and breast properties at their interface [see Figure 1(a)] when this boundary resides within the imaging zone. The idea of conforming the mesh to the exact breast perimeter allows us to apply a property step function at the object coupling-mediuminterface in the forward solution to accurately imitate the experimental configuration [see Figure 1(b)] and eventually reduce the smoothing effects due to the high contrast at the object perimeter. Finally, this concept also enables us to improve the correlation analysis procedure with images from the NIR and EIS breast imaging systems. These modalities are contacting imaging systems where the breast is illuminated via direct contact of the optical fibers or electrodes, respectively. The recovered property distributions in those mo dalities represent only the area containing the breast. Therefore, it will be easier to compare NIR and EIS images with the microwave results using the conformed imaging domain technique than with the original antenna-concentric perimeter mesh.

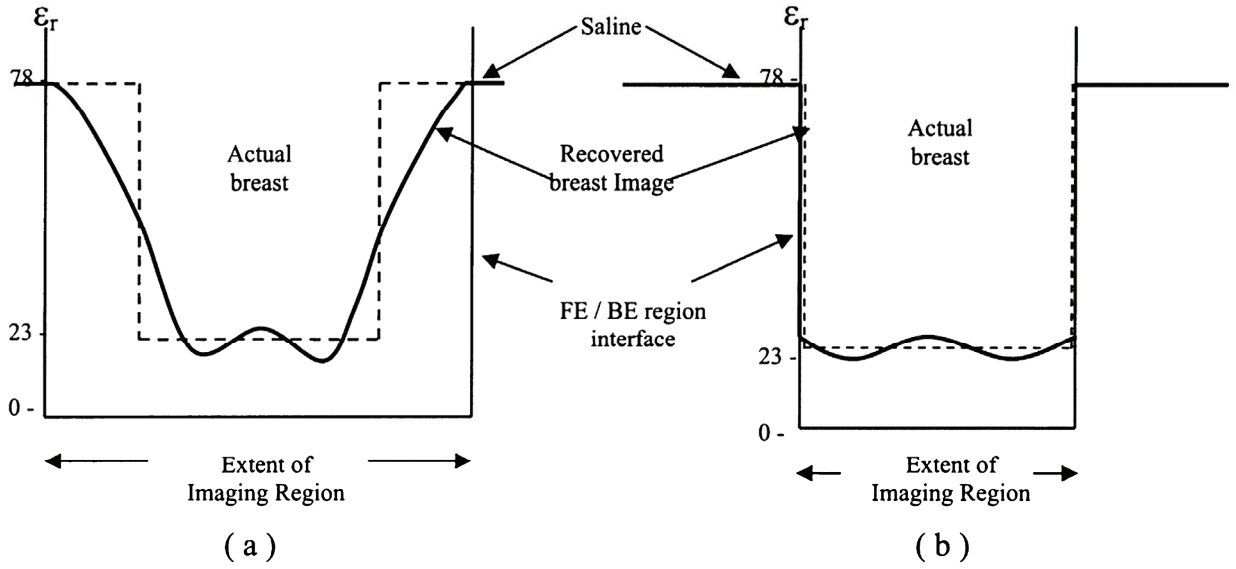

Figure 1. Conceptual illustration of relative permittivity profile of actual breast and reconstructed breast in saline background medium for the: (a) concentric mesh, which also contains portions of saline background and (b) conformal mesh,which contains only the imaged breast.

2.2. Phantom Fabrication and Data Acquisition System

Phantom experiments were performed using agar gel with varying concentrations of low dielectric solutions mixed with agar powder to control the relative permittivity. The most convenient low-permittivity liquid was corn syrup with ε_r=13 and σ=0.2S/m at 900MHz.M ixtures of corn syrup and water in varied proportions can be produced with ε_r ranging from 13 at the low end to 77 in liquid form. However, because the ability of agar to gel degrades significantly at higher corn-syrup proportions, a practical lower bound on the permittivity of the gel is roughly ε_r=35 at 900MHz. These values are higher than published data for ex vivo breast permittivities; however, in terms of assessing the capabilities of this newgeneral approach, the properties are adequate. The recipe for this phantom material was 78% corn syrup, 21% water, and 1% agar, which produced a gel with ε_r=35 and σ=0.7S/m at 900MHz. The gel was formed in a 1000-mL glass beaker heated to 120° C for 40 min in an autoclave. The electrical properties were measured by using an Agilent 85070B Dielectric Probe Kit in the conjunction with an Agilent 8753C Network Analyzer. It should be noted that the gelling action had the unwanted consequence of significantly increasing the conductivity with respect to the initial liquidmix-ture, which was considerably higher than the values reported for the breast. Subsequently, we have not only included simulation experiments, which mimic those agar gel values, but have also presented data for cases that more closely represent published breast properties in Section 3. Phantom experiments and breast examinations were performed using the clinical prototype microwave imaging system fabricated by Meaney *et al*. [4]. It is a saline-coupled noncontacting clinical interface with a 16-monopole-antenna array operating over a broad bandwidth of 300–1000 MHz. Data (electric-field magnitude and phase) are collected at 144 (16 transmitters ×9 receivers per transmitter) measurement sites as inputs for the HE element image-reconstruction algorithm.

3. Results

For the purpose of exploring the feasibility of this new approach, the conformal-imaging scheme was initially evaluated in simulation and phantom tests with known boundaries. Following that, a complete two-step conformal-imaging process is demonstrated in a patient breast exam where the precise breast/background interface is unknown. Finally, additional simulation studies are included to demonstrate that the image recovery improves progressively as the mesh approaches the actual target contour, which occurs for both high- and low-contrast backgrounds. This provides a guide for determining the accuracy of the target contour needed to achieve a certain degree of image-quality improvement. Results presented in these sections compare images obtained with the fixed mesh and the new conformal-domain approaches. It should be noted that the results shown here only included image data at 900 MHz, but that similar findings have been observed over the spectral range of 300–1000 MHz.

3.1 Imaging-Reconstruction Scheme

1) Simulations: Simulation experiments presented here were performed at 900 MHz with a saline background medium having ε_r=77 and σ=1.6SS/m. An 8.2-cm-diameter object was placed centrally within an imaging array

with electrical properties of ε_r=35 and σ=0.7S/m. To simulate the problem of detecting a tumor-like abnormality within a breast, we have inserted a 1.9-cm-diameter inclusion offset 2.3 cm from the center with electrical properties identical to the background medium. Note that using saline as the inclusion approximates the contrast ratio that may be presented in an actual breast with a tumor based on *ex vivo* electrical property studies [8–10]. Figure 2(a) and (b) shows the recovered relative permittivity (left-hand side) and conductivity (ri- ght-hand side) images for the cases with the general concentric and conformed domain mesh, respectively. Longitudinal transects (relative permittivity and conductivity counterparts) of these images are presented in Figure 2(c). Comparisons are performed between the actual and reconstructed values for the two mesh approaches.

The images in Figure 2(a) show the cylindrical object with gradual property gradients at the object/saline interface for both permittivity and conductivity cases. The saline inclusion is, at best, discernible only as a minor perturbation in the right of the object perimeter. Correspondingly smooth profiles [solid plus lines in Figure 2(c)] provide little information about the presence of the heterogeneity, except for the fact that longitudinal transects of the distributions through the actual inclusion appear slightly asymmetric. The images using the conformal mesh approach present a much different picture. They reveal a uniform ε_r distribution excluding a significant property increase corresponding to the saline inclusion location and a conductivity counterpart with similar behavior where the inclusion is again quite obvious. An important feature illustrated here is that the large low-permittivity object appears to be smaller in the conductivity image than the corresponding permittivity image. This accounts for the appearance of some gradients surrounding the periphery of the conductivity object evenwith the conformal mesh technique. Generally, proper ties are recovered more accurately with the conformal mesh method than with the fixed concentric mesh approach.

2) Phantom Experiments: Figure 3 shows the imaging results for the same case demonstrated in Figure 2, except using actual measured data. The longitudinal transects through the property distributions of the recovered

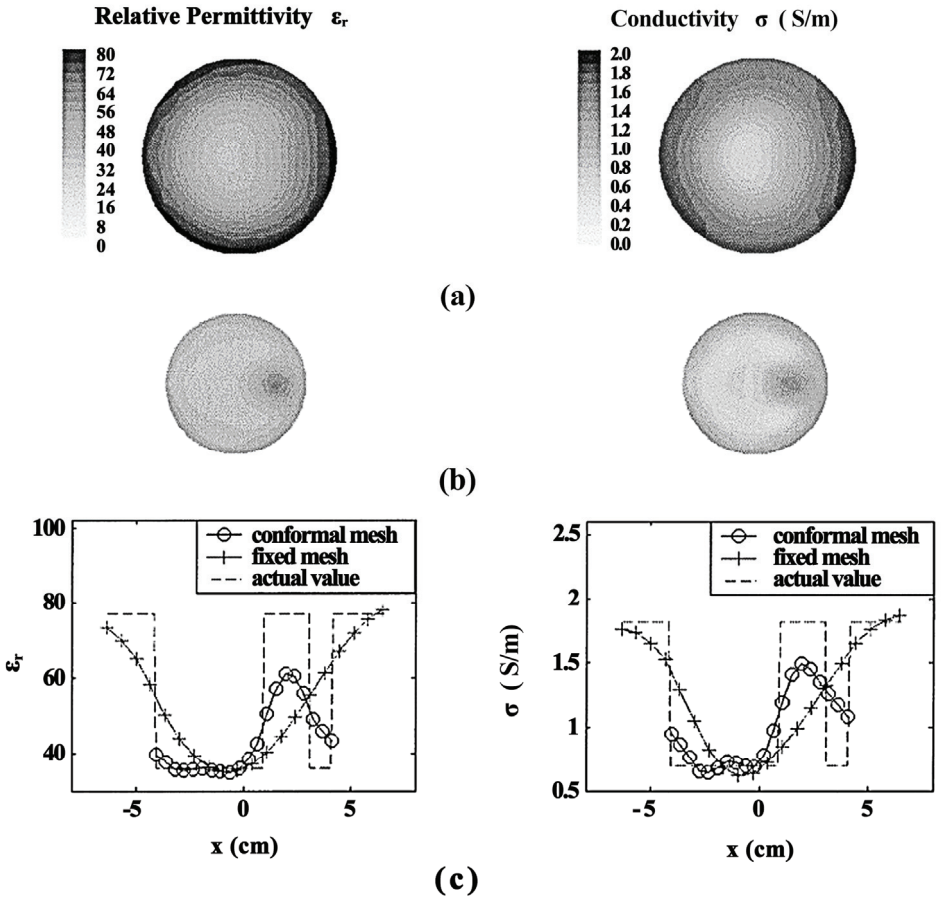

Figure 2. 900-MHz reconstructed images of a simulated 8.2-cm-diameter breast equivalent object with a 1.9-cm-diameter-tumor inclusion for two different FE meshes. (a) Fixed concentric FE mesh. (b) Conformal FE mesh. (c) Electric property profiles along longitudinal transects through the object and inclusion. In the conformal mesh case, transects terminate at the actual breast object/background interface

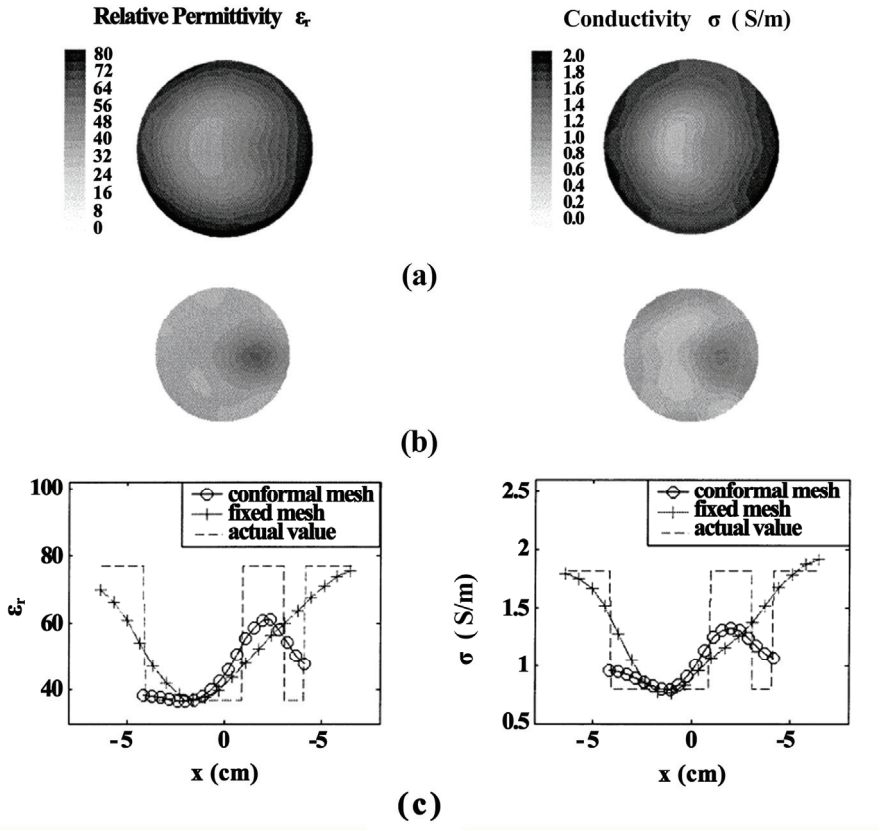

Figure 3. 900-MHz reconstructed images of a 8.2-cm-diameter agar phantom with a 1.9-cm-diameter tumor inclusion for two different FE meshes using measured data. (a) Fixed concentric FE mesh. (b) Conformal FE mesh. (c) Electric property profiles along longitudinal transects through the object and inclusion

object are far closer to the actual profile for the conformal mesh approach. For the general fixed-mesh approach, shown in Figure 3(a), very smooth images were recovered similarly to the previous simulation results in Figure 2(a), which indicate good consistency between the measured and simulated data. As in the simulation study, the object in the conductivity image is smaller than its permittivity counterpart, which is also the case with the general concentric mesh approach. This produces a ring of slightly higher conductivity surrounding the image. Despite the ring effect, the conformal mesh image is quite uniform, except for the inclusion, and clearly contains more information than the image from the general concentric mesh case.

3.2. Initial Patient Exam

Similarly to the phantom results of Section III-A.2, Figure. 4(a) and (b) shows the en face reconstructed images for the first three antenna positions (at 1-cm increments with position 1 being closest to chest wall) of the 900-MHz right-breast exam of a 36-year-old patient using the fixed and conformal mesh imaging approaches, respectively. The patient had ra- diographically dense breasts and an ultrasound exam detected a 17-mm-diameter mass in the outer right breast, closer to the nipple. Due to the difficulty in determining the exact breast perimeter, a best-fitting ellipse (determined empirically) was chosen for each conformal mesh image plane. As with the phantom cases, the recovered images using the general concentric mesh are very smooth over the breast/coupling medium interface, and suggest only a minor indentation on the left-hand side near the breast perimeter. However, these images do provide qualitative breast perimeter information at eac position with which conformal meshes can be constructed. The solid elliptical traces superimposed on the images in Fig. 4(a) define estimated breast/saline-solution interfaces over which the new conformed mesh image is computed. Observations are consistent with the previous phantom experiments in that the images are enhanced and the mass is detected in the upper outer quadrant where a significant localized ε_r increase occurs compared with the rest of the relatively uniform breast. Unlike the phantom experiment, the conductivity images do not demonstrate significant improvement using the conformal mesh approach in this case, which may be the result of increased three-dimensional (3-D) wave propagation effects that are exacerbated in this instance since the breast does not generally resemble a semi-infinite cylinder, as in the phantom experiments. It is interesting to note the appearance of slightly decreased permittivity around the edge of the position-3 images using the conformal mesh. In general,

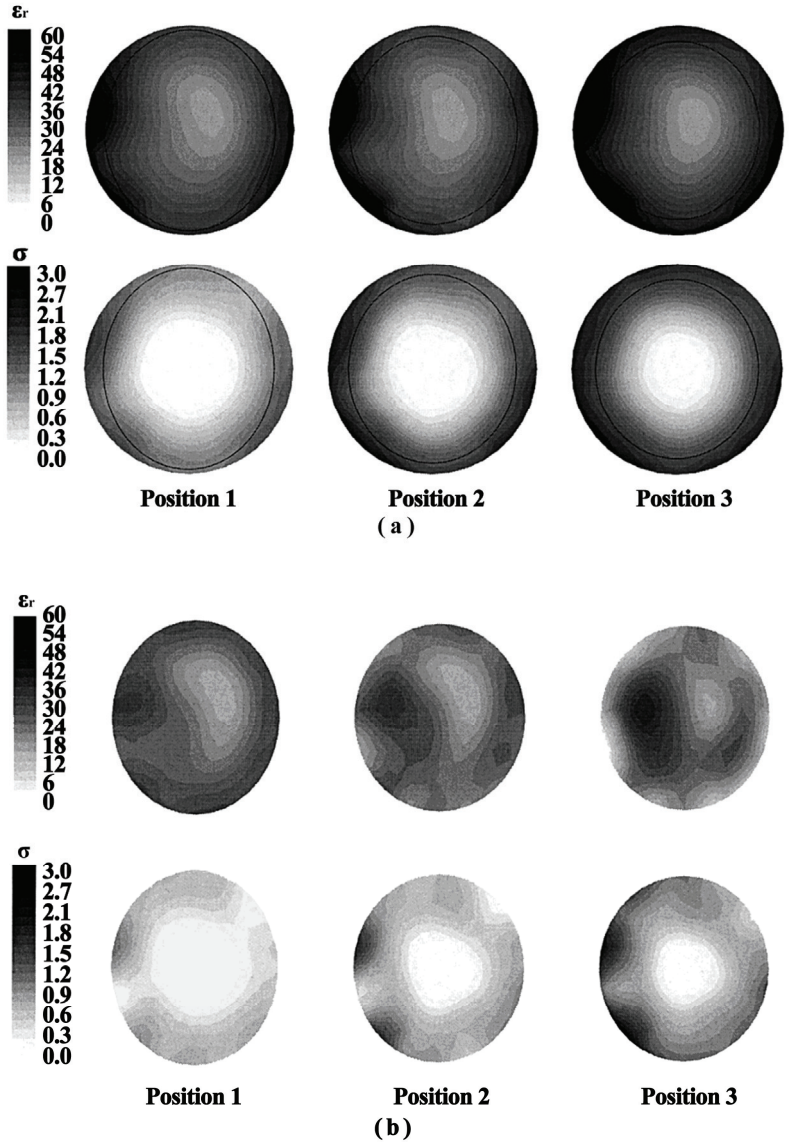

Figure 4. 900-MHz reconstructed permittivity and conductivity images for three different antenna array positions for the right breast of the 36-year-old patient using: (a) the fixed concentric mesh and (b) the conformal mesh.

the appearances of these effects indicate that the mesh was reduced too much in size, allowing the mesh perimeter to reside partially in the tissue area instead of solely in the background medium. Nonetheless, the improvements in the permittivity images are significant.

3.3. Mesh Boundary Convergence

In this study, a 2-D simulated elliptical breast cross section with 10-cm major and 8-cm minor axes, respectively, was centered within the array. It was oriented at 20° with respect to the horizontal axis to accentuate its nonuniform (i.e., not circular) geometry in the image field of view. To facilitate systematic studies on image quality as the reconstructionmesh converges to the exact breast boundary, a series of images were recovered on reconstruction meshes consisting of different sized ellipses: (a) 13×11 cm, (b) 12×10 cm, (c) 11×9 cm, and (d) 10×8 cm, with the major axes of each oriented identically to that of the actual breast phantom. The properties used for the breast were ε_r=23 and σ=0.18S/m, respectively. Additionally, to facilitate the study of image artifacts as a function of breast/background mediumcontrast, a range of background relative permittivities were used: ε_r=80 and 40 (with a fixed conductivity of 1.7 S/m) in order to demonstrate the robustness of the conformal mesh approach in both low- and high-contrast situations. A second set of simulation experiments were performed for the same object and background media, except for a 1.9-cm-diameter tumor inclusion with electrical prope ties of ε_r=57 and σ=1.18S/m.

Figure 5(a) shows the sequence of recovered images for the homogeneous breast phantom for the four reconstruction meshes with a high contrast background (ε_r=8

0). The gradient surrounding the object perimeter is considerably diminished as the mesh approaches the breast. A similar set of images for the breast with tumor inclusion [see Figure 5(c)] demonstrates increased resolution of the tumor as the mesh approaches the breast , which is consistent with the simulation results in Section III-A. Note that, in all cases, there are undesired artifacts in both image components. Figure 5(b) and (d) shows a similar sequence of images for the same reconstruction-meshes, but with a much lower background contrast (ε_r=40).It is clear that, in all cases, especially for those where the mesh more closely matches the actual breast size, that the artifacts are considerably less discernible. This observation is also confirmed in the set of profile comparisons between the actual and recovered values when using the two different background media [see Figure 5(e) and (f)], where the properties within the object boundaries for the lower contrast background deviate

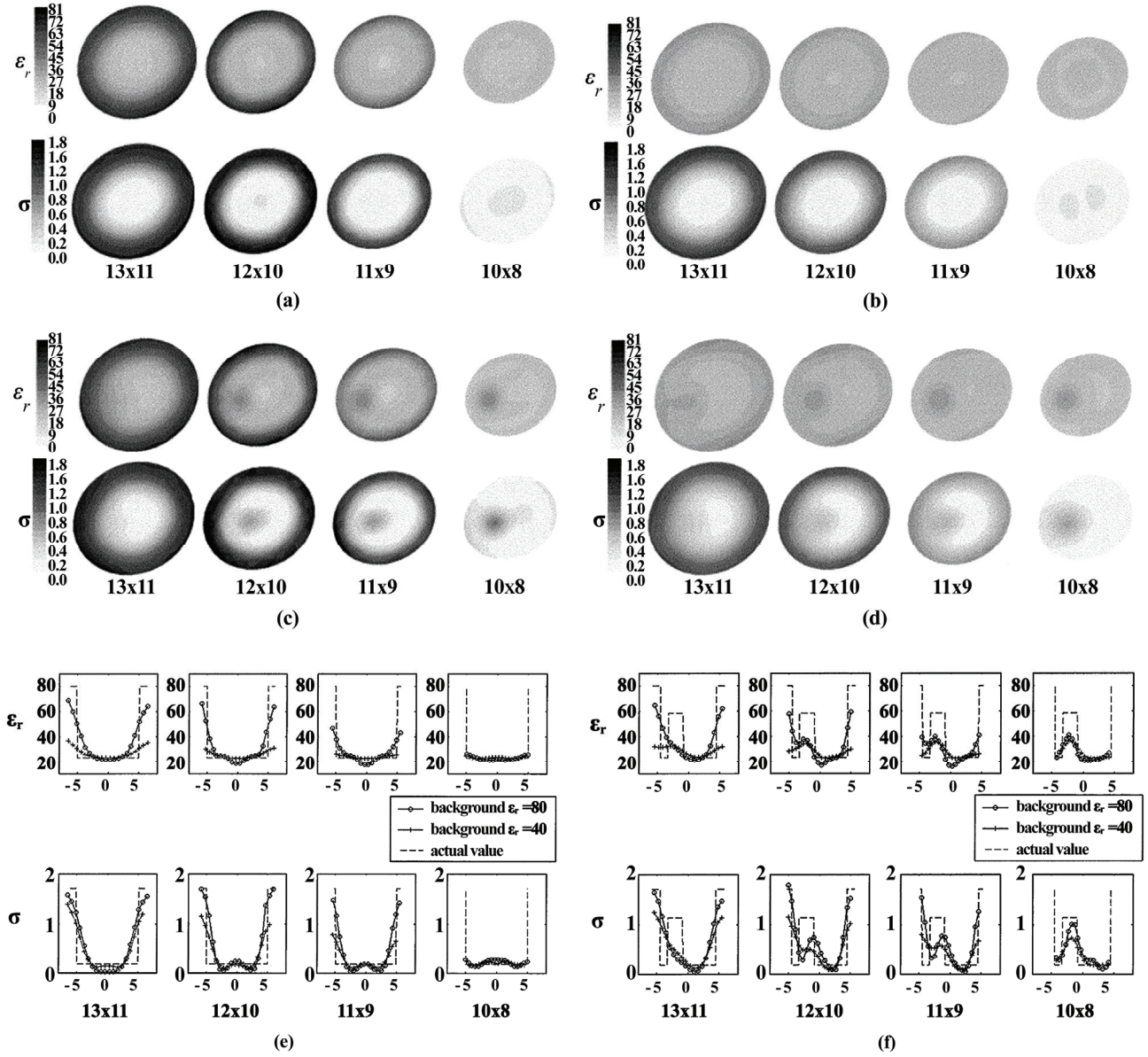

Figure 5. (a) 900-MHz reconstructed permittivity and conductivity images for a 10×8 cmhomogeneous elliptical breast cross section using different reconstruction meshes with a background medium having ε_r=80 and α=107 S/m. (b) 900-MHz reconstructed permittivity and conductivity images for a 10×8cm homogeneous elliptical breast cross section using different reconstruction meshes with a background medium having ε_r=40 and α=1:7 S/m. (c) 900-MHz reconstructed permittivity and conductivity images for a 10×8 cm elliptical breast cross section with tumor-like inclusion using different reconstruction meshes with a background medium having ε_r=80 and α=1:7 S/m. (d) 900-MHz reconstructed permittivity and conductivity images for a 10×8 cm elliptical breastcross section and tumor-like inclusion using different reconstruction meshes with a background medium having ε_r=40 and α=1:7 S/m. (e) 900-MHz electric property profile along the major axes through the different-sized reconstruction meshes for the homogeneous elliptical breast. (f) 900-MHz electric property profile along the inclusion-origin center line through the different sized reconstruction meshes for the elliptical breast with tumor-like inclusion

less from their true value. For the cases where the mesh is physically larger than the breast, a considerable portion of the profile with a high-contrast background is engaged in representing the steep gradient between the background medium and breast. Additionally, in Figure 5(f), for the larger mesh cases and both backgrounds, the recovered inclusion location in the conductivity images is misaligned somewhat with respect to the actual location. As the mesh size is gradually conform to the breast perimeter, the recovered inclusion location improves considerably. This illustrates that the image quality can be improved significantly even with only a good estimate of the object boundary. (In practice, it may prove difficult to define the exact object contour.) This observation appears to be consistent for both the high- and low-contrast situations.

4. Conclusions

Our model-based noncontacting microwave imaging system allows for an arbitrarily shaped imaging domain within the antenna array. Using a Gauss–Newton iterative image-reconstruction approach based on a hybrid of the FE and BE methods, we have shown that it is feasible to conform the imaging domain to or close to the actual target tissue. This facilitates deployment of the reconstruction parameters solely to the zone occupied by the oject, which can improve spatial resolution considerably.

Implementation of the conformal-imaging approach involves two steps, i.e., identifying the imaging object boundary and recovering its dielectric properties on the conformal mesh. Provided that the boundary can be identified, the reconstruction can be performed in a similar fashion as the fixed concentric mesh method. Currently, two strategies have been suggested for localizing the object/saline interface based on our existing data acquisition system. The first strategy utilizes projection information of the measured electric-field magnitude and phase to construct an approximate perimeter as the imaging object is illuminated by the transmitted microwave signals from multiple directions. This requires additional boundary information preprocessing, but generally consumes only a small portion of the computation time when compared with the overall reconstruction costs. The second strategy defines the target boundary by analyzing the image recovered on the fixed concentric mesh, essentially creating a two-step image-reconstruction scheme where breast boundary information is derived from the images obtained in the first step. This was the procedure used in the patient exam described in Section III-C. We have presented results here that demonstrate the feasibility of the imaging approach and have left the task of implementing an automated procedure for identifying the breast/background boundary for further investigation.

Implementation of the conformal mesh facilitates a property step function at the breast background interface, which accurately mimics the signal illumination condition of the breast within the antenna array. In this way, the problem of recovering the step gradients at the object perimeter is eliminated and more reconstruction parameters can be deployed to representing the object property distributions. Additionally, removal of the gradients on the image perimeter will enhance correlation of these images with the other alternative imaging modalities being developed at Dartmouth College (NIR and EIS),which utilize contacting fiber cables or electrodes and do not take into account the fields outside of the breast.

Although we have also observed object artifacts in some homogenous phantom images that could be interpreted as false positive detections in an actual patient examination, simulation results presented here illustrate that, if the electrical property contrast between the background medium and breast is reduced, the conformal mesh approach can be used successfully with only minimal artifacts while retaining the improved inclusion detection characteristics associated with the conformal mesh technique. Related improvements afforded by reducing the background contrast have also been observed in a recent study of 3-D artifacts (controlled experiments utilizing our 2-D imaging system to image 3-D targets such as spheres and cones) [25].

REFERENCES

[1] A. G. R. Lynn, L. Carol, B. Kosary, and F. Hankey, "SEER cancer statistics review 1973–1994," Nat. Cancer Inst., Bethesda, MD, NIH Pub. 2789, 1997.

[2] M. Brown, F. Houn, E. Sickles, and L. Kessler, "Screening mammography in community practice," Amer. J. Radiol., vol. 165, pp. 1373–1377, 1995.

[3] P. T. Huynh, A. M. Jarolimek, and S. Daye, "The false-negative mammogram," Radiographics, vol. 18, no. 5, pp. 1137–1154, 1998.

[4] P. M. Meaney, M. W. Fanning, D. Li, S. P. Poplack, and K. D. Paulsen, "A clinical prototype for active microwave imaging of the breast," IEEE Trans. Microwave Theory Tech., vol. 48, pp. 1841–1853, Nov. 2000.

[5] T. E. Kerner, "Electrical impendence tomography for breast imaging," Ph.D. dissertation, Thayer School of Eng., Dartmouth College, Hanover, NH, 2001.

[6] T. O.McBride, "Spectroscopic reconstructed near infrared tomographic imaging for breast cancer diagnosis," Ph.D. dissertation, Thayer School of Eng., Dartmouth College, Hanover, NH, 2001.

[7] E. E.W. Van Houten, K. D. Paulsen,M. I.Miga, F. E. Kennedy, and J. B. Weaver, "An overlapping subzone technique for MR based elastic property reconstruction," Magn. Resonance in Med., vol. 42, pp. 779–786,1999.

[8] R. K. M. Chaudhary, A. Swarup, and J. M. Thomas, "Dielectric properties of normal and malignant human breast tissues at radiowave and microwave frequencies," Indian J. Biochem. Biophys., vol. 21, pp. 76–79, 1984.

[9] C. Gabriel, S. Gabriel, and E. Corthour, "The dielectric properties of biological tissues," Phys. Med Biol., vol. 41, pp. 2231–2249, 1996.

[10] W. T. Joines, Y. Zhang, C. Li, and R. L. Jirtle, "The measured electrical properties of normal andmalignant human tissues from50 to 900MHz," Med. Phys., vol. 21, pp. 547–550, 1994.

[11] V. G. Peters, D. R. Wyman, M. S. Patterson, and G. L. Frank, "Optical properties of normal and diseased breast tissue in the visible and near infrared," Phys. Med. Biol., vol. 35, pp. 1317–1334, 1990.

[12] T. A. Krouskop, T. M. Wheeler, F. Kallel, B. S. Ciarra, and T. Hall, "Elastic moduli of breast and prostate tissue under compression," Ultrason. Imaging, vol. 20, pp. 260–274, 1998.

[13] K. L. Carr, "Microwave radiometry: Its importance to the detection of cancer," IEEE Trans. Microwave Tech., vol. 37, pp. 1862–1896, Dec. 1989.

[14] B. Bocquet, R. Ait-Abdelmalek, A. Mamouni, K. Ridaoui, and Y. Leroy, "Influence of the permittivity of breast tissues on the robust of microwave radiometric imaging," in Application of Microwaves in Medicine, ser. IEEE Collections. Piscataway, NJ: IEEE Press, 1995, pp. 6/1–6/5.

[15] S. C. Hagness, A. Taflove, and J. E. Bridges, "Two-dimensional FDTD analysis of a pulsed microwave confocal system for breast cancer de tection: Fixed-focus and antenna-array sensors," IEEE Trans. Biomed. Eng., vol. 45, pp. 1470–1479, Dec. 1998.

[16] E. C. Fear and M. A. Stuchly, "Microwave detection of breast cancer," IEEE Trans. Microwave Tech., vol. 48, pp. 1854–1863, Nov. 2000.

[17] S. Caorsi, G. L. Gragnani, and M. P. Pastorino, "Reconstruction of dielectric permittivity distributions in arbitrary 2Dinhomogeneous biological bodies by a multiview microwave numerical method," IEEE Trans.Med. Imag., vol. 12, pp. 1742–1752, June 1991.

[18] A. E. Souvorov, A. E. Bulyshev, S. Y. Semenov, R. H. Svenson, and G. P. Tatsis, "Two-dimensional computer analysis of amicrowave flat antenna array for breast cancer tomography," IEEE Trans.Microwave Tech., vol. 48, pp. 1413–1415, Aug. 2000.

[19] L. Jofre, M. S. Hawley, A. Broquetas, E. de los Reyes, M. Ferrando, and A. R. Elias-Fuste, "Medical imaging with a microwave tomographic scanner," IEEE Trans. Biomed. Eng., vol. 37, pp. 303–312, Mar. 1990.

[20] Z. Q. Zhaug and Q. H. Liu, "Microwave imaging for breast tumor; 2D forward and inverse methods," in IEEE AP-S Int. Symp., vol. 1, 2001, pp. 242–245.

[21] P. M. Meaney, K. D. Paulsen, and T. P. Ryan, "Two-dimensional hybrid element image reconstruction for TM illumination," IEEE Trans. Antennas Propagat., vol. 43, pp. 239–247, Mar. 1995.

[22] K. D. Paulsen, P. M. Meaney, M. J. Moskowitz, and J. M. Sullivan, "A dual mesh scheme for finite element based reconstruction algorithms," IEEE Trans. Med. Imag., vol. 14, pp. 504–514, Sept. 1995.

[23] G. A. F. Seber and C. J.Wild, Nonlinear Regression. New York:Wiley, 1989, pp. 619–660.

[24] P. M. Meaney, E. Demidenko, N. K. Yagnamurthy, D. Li, M. W. Fanning, and K. D. Paulsen, "A two-stage microwave image reconstruction procedure for improved internal feature extraction,"Med. Phys., vol. 28, pp. 2358–2369, 2001.

[25] P. M. Meaney, S. A. Pendergrass, M. W. Fanning, N. K. Yagnamurthy, and K. D. Paulsen, "Importance of using a reduced contrast coupling medium in 2D microwave breast imaging," J. Electromagn. Waves Applicat., 2003, to be published.

